Energy analysis of substorms based on remote sensing techniques, solar wind measurements, and geomagnetic indices

N. Østgaard,[1,2] G. Germany,[3] J. Stadsnes,[4] and R. R. Vondrak[5]

Received 21 June 2001; revised 30 October 2001; accepted 9 November 2001; published 12 September 2002.

[1] Observations from the Polar Ionospheric X-ray Imaging Experiment (PIXIE) and the Ultraviolet Imager (UVI) on board the Polar satellite have been used to examine the energy deposition in the Northern Hemisphere by precipitating electrons for seven substorms during 1997. By combining the results from these two remote sensing techniques we derive the 5 min average electron energy distributions from 100 eV to 100 keV with a spatial resolution of ~700 km. During growth phase we find that most of the energy is carried by electrons below 10 keV. The study shows that the maximum intensity of the substorm is mostly defined by the flux of electrons below 10 keV. In contrast, the electrons above 10 keV show a greater intensification at substorm onset and are more confined azimuthally during the expansion phase. By using the most appropriate parameterized methods to estimate the energy increase of the ring current (U_R) and the Joule heating rate in both hemispheres (U_J) and by adding the rate of energy deposition in both hemispheres by precipitating electrons (U_A), we estimate the total energy dissipation rate during substorms (U_T). Our estimate of U_A is a factor 2–4 larger than that reported in earlier studies. We find that the contributions to the total time-integrated energy dissipation over the duration of the substorm, $W(U_T)$, from $W(U_R)$, $W(U_J)$, and $W(U_A)$ on average are 15%, 56%, and 29%. Comparing $W(U_T)$ and the time-integrated ϵ parameter, $W(\epsilon)$, which approximates the solar wind input due to dayside reconnection, we find that the ϵ parameter does not always provide enough energy into the magnetosphere to balance $W(U_T)$. An additional energy transfer mechanism is needed to balance the energy budget. We find that a viscous interaction that transfers 0.17% of the solar wind kinetic energy in addition to the energy transfer due to dayside reconnection, estimated by the ϵ parameter, is sufficient to balance the total energy dissipation U_T. *INDEX TERMS:* 2784 Magnetospheric Physics: Solar wind/magnetosphere interactions; 2736 Magnetospheric Physics: Magnetosphere/ionosphere interactions; 2455 Ionosphere: Particle precipitation; 2716 Magnetospheric Physics: Energetic particles, precipitating; *KEYWORDS:* energy budget of substorms, X-ray and UV imaging, particle precipitation, Joule heating, ring current, solar wind

Citation: Østgaard, N., G. Germany, J. Stadsnes, and R. R. Vondrak, Energy analysis of substorms based on remote sensing techniques, solar wind measurements, and geomagnetic indices, *J. Geophys. Res.*, *107*(A9), 1233, doi:10.1029/2001JA002002, 2002.

1. Introduction

[2] Plasma erupted from the Sun, carrying the interplanetary magnetic field, can penetrate the magnetic shielding of the Earth through a reconnection process. This merging of field lines and penetration of particles represent an energy transfer into the magnetosphere. The energy can then either be deposited "directly" into the ionosphere with a typical delay of ~20 min or be stored in the magnetosphere and with a typical delay time of ~60 min be dissipated during substorms [*Bargatze et al.*, 1985; *Tsurutani et al.*, 1985; *Liou et al.*, 1998]. These two categories of energy deposition events are usually referred to as directly driven events and loading-unloading events [see, e.g., *Baker et al.*, 1984; *Rostoker*, 1991; *Elphinstone et al.*, 1996]. The directly (solar wind) driven processes can be convection events with no subsequent substorm or convection signatures prior to the substorm breakup during the substorm growth phase [*Baker et al.*, 1997]. The loading-unloading event refers to the storing of energy during growth phase and the abrupt substorm breakup followed by a global expansion of the auroral oval.

[3] *Perrault and Akasofu* [1978] and *Akasofu* [1981] examined magnetic storms and substorms to estimate the

[1]Department of Physics, University of Oslo, Oslo, Norway.
[2]Now at Laboratory for Extraterrestrial Physics, Goddard Space Flight Center, Greenbelt, Maryland, USA.
[3]Center for Space Plasma and Aeronomy Research, University of Alabama in Huntsville, Huntsville, Alabama, USA.
[4]Department of Physics, University of Bergen, Bergen, Norway.
[5]Laboratory for Extraterrestrial Physics, Goddard Space Flight Center, Greenbelt, Maryland, USA.

0148-0227/02/2001JA002002$09.00

different forms of ionospheric and magnetospheric energy dissipation. Based on these estimates they derived the Akasofu energy input parameter ϵ. This is a semiempirical function which has been shown to approximate the solar wind energy input to the magnetosphere due to dayside reconnection. The three most important forms of ionospheric and magnetospheric energy dissipation are the energy increase of the ring current (U_R), the Joule heating of the atmosphere (U_J) and the particle precipitation (U_A) [*Akasofu*, 1981; *Baker et al.*, 1997; *Knipp et al.*, 1998], although other forms of energy dissipation like the plasma sheet heating and the energy returned to the solar wind by plasmoid ejections from the tail might be considered as well [*Baker et al.*, 1997; *Ieda et al.*, 1998; *Lu et al.*, 1998].

[4] During magnetic disturbed conditions particle injections in the tail can lead to an intensification of the ring current, which can be monitored as geomagnetic disturbances at low latitudes. Four stations near the equator have therefore been selected to provide a global index (*Dst*) for the ring current [*Sugiura*, 1964]. Several studies have shown that the pressure corrected *Dst* (*Dst**) index can be used to estimate U_R [*Perrault and Akasofu*, 1978; *Akasofu*, 1981; *Zwickl et al.*, 1987; *Gonzalez et al.*, 1994]. A more accurate estimate of U_R has been suggested by differentiating the values for the ring current life time [*Prigancova and Feldstein*, 1992; *Gonzalez et al.*, 1994; *Lu et al.*, 1998].

[5] The Joule heating which is controlled by the Pedersen currents and the electric field has been found to be closely related to the *AE* index [*Perrault and Akasofu*, 1978; *Akasofu*, 1981; *Ahn et al.*, 1983, 1989; *Baumjohann and Kamide*, 1984; *Richmond*, 1990; *Cooper et al.*, 1995; *Lu et al.*, 1995, 1998]. Seasonal and hemispherical differences have been examined as well to establish a more accurate relation between U_J and the geomagnetic indices [*Nisbet*, 1982; *Lu et al.*, 1998]. However, most of the relations do not take into account the neutral wind effect, which can affect the estimate of U_J significantly [*Lu et al.*, 1995; *Emery et al.*, 1999].

[6] As particle precipitation through ionization affects the Hall conductance and thereby increases the Hall currents resulting in disturbances of the geomagnetic field, U_A is believed to be related to the *AE* (or *AL*) indices [*Akasofu*, 1981; *Spiro et al.*, 1982; *Ahn et al.*, 1983; *Richmond*, 1990; *Lu et al.*, 1998; *Østgaard et al.*, 2002]. Where instantaneous global measurements of electron precipitation are not available, the U_A have to be derived indirectly from radars or magnetic data or from statistical particle measurements by low-altitude satellites. In a companion paper [*Østgaard et al.*, 2002] we discuss the accuracy of these estimates.

[7] A general understanding of the energy flow from the solar wind to the magnetospheric-ionospheric system is given by *Stern* [1984], which also presents some typical values of the different forms of energy during disturbed magnetic conditions. In a review paper on magnetic storms *Gonzalez et al.* [1994] discuss the different forms of energy and also present the different energy coupling functions between the solar wind and the magnetosphere. Recently there have been some studies that examine qualitatively the total energy budget and/or the different energy depositions in the ionosphere. *Lu et al.* [1995] used the National Center for Atmospheric Research thermosphere-ionosphere general circulation model (NCAR TIGCM) and the assimilative mapping of ionospheric electrodynamics (AMIE) procedure to examine the effect of neutral winds on the U_J during the Geospace Environment Modeling (GEM) campaign period: March 28–29, 1992. They also calculated the ratio U_J/U_A during that period. As a part of a comprehensive study of a severe magnetic storm 2–11 November, 1993, *Knipp et al.* [1998] utilized a huge database to estimate both ϵ, U_{SW}, U_R, U_J and U_A and presented a total energy budget for the entire storm period. The same storm period was studied by *Emery et al.* [1999] to examine the thermospheric neutral response to the magnetic storm. Using the TIGCM and AMIE procedures they estimated the neutral wind effect on the U_J, the seasonal variations of U_J as well as the ratio U_J/U_A. Also, *Lu et al.* [1998] used a comprehensive set of data to study the total energy budget for the magnetic cloud event on January 10–11, 1997. They used the AMIE procedure supported by auroral electron energy fluxes derived from ultraviolet (UV) images to estimate both U_R, U_J and U_A during this event. *Liou et al.* [1998] used the UV images from Polar to estimate the energy deposition by precipitation. *Kallio et al.* [2000] used the local AL index from the International Monitor for Auroral Geomagnetic Effects (IMAGE) as input to the relation found by *Ahn et al.* [1983] to presented statistical results of the Joule heating during growth phase and expansion phase of substorms compared with the solar wind input estimated by the ϵ parameter.

[8] In this study we have used the combined measurements from the Polar Ionospheric X-ray Imaging Experiment (PIXIE) [*Imhof et al.*, 1995] and the Ultraviolet Imager (UVI) [*Torr et al.*, 1995] to derive the 5 min average precipitating electron energy distribution from 100 eV to ~100 keV with a spatial resolution of ~700 km on a global scale during 7 substorms. This method was examined by *Østgaard et al.* [2001] and was found to give a fairly precise estimate of the energy deposition by auroral electrons. The focus of the study in this paper is twofold. (1) We examine how the hemispherically integrated energy input by the various energy regimes of electrons, i.e., above and below 10 keV, behaves during substorms. (2) By using the ϵ parameter to estimate the solar wind energy input and using the most appropriate parameterized methods to derive U_R and U_J we estimate the total energy budget for these substorms. We discuss the different parameterized methods to derive U_R and U_J, as well as the advantage of using multispectral imaging techniques to derive U_A. In a companion paper using the same data set we show how the U_A is related to the geomagnetic indices *AE*, *AL* and *AU* [*Østgaard et al.*, 2002].

2. Instrumentation and Data Processing

[9] PIXIE is a pinhole camera providing X-ray measurements in the energy range ~3–22 keV. When the Polar satellite is at apogee we get global X-ray images with a spatial resolution of ~700 km. Due to an intermittent high voltage supply problem the PIXIE instrument has been duty cycled. During the events used in this study, the duty cycling was 5 min on and 10 min off. The X rays measured by PIXIE are produced by electrons from ~3 keV to 100 keV. Detailed descriptions of the data processing from PIXIE is given by *Østgaard et al.* [1999] and details on deriving four-parameter electron spectra from PIXIE meas-

urements are given by *Østgaard et al.* [2000] and *Østgaard et al.* [2001].

[10] The UVI provides global images of ultraviolet emissions in the Lyman-Birge-Hopfields (LBH) band. The UVI instrument makes two separate measurements within the LBH band, the LBH short and LBH long. Emissions in the LBH long band is approximately proportional to the total energy flux of electron precipitation below ~20–50 keV and, as the UV emissions within LBH long and LBH short are differently affected by the absorption by molecular oxygen, the measurements can be used to derive spectral information about the parent electrons. As pointed out by e.g., *Frey et al.* [2001] the emission lines within the LBH band are also produced by proton precipitation that might be important under certain circumstances. A detailed description of the technique used to derive a two-parameter electron spectrum from the UVI measurements is given by *Germany et al.* [1997, 1998a, 1998b].

[11] The solar wind density and velocity and measurements of the interplanetary magnetic field (IMF), with a time resolution of 79 s and 46 s, respectively, were available from the solar wind experiment [*Ogilvie et al.*, 1995] and the magnetic field experiment [*Lepping et al.*, 1995] on board the Wind spacecraft.

[12] The quick look AE_{QL}, AU_{QL} and AL_{QL} indices, 1 min resolution were available from the World Data Center for Geomagnetism, Kyoto, Japan and are based on 6–8 of the 12 standard stations during the events used in this study, except for one event (July 31, 1997) where only 4 stations were included. The advantage of choosing the quick look geomagnetic indices is that they are easily accessible, but it requires that one must make certain that the few stations are well located regarding the regions of intense electron precipitation.

[13] By combining the measurements from UVI and PIXIE it is possible to derive 5 min-average electron distributions from 100 eV to 100 keV with a spatial resolution of ~700 km in the Northern Hemisphere when Polar is at 6–8 R_E. A validation of the method by comparing with directly measured electron spectra by low-altitude satellites is given by *Østgaard et al.* [2001]. The time resolution of 15 min (5 min-average every 15 min) is determined by the duty cycling of the front chamber of PIXIE and the spatial resolution is basically determined by the pinhole size of the PIXIE instrument. For details about how wobbling of the despun platform and the satellite movement affect the spatial resolution we refer to *Østgaard et al.* [2001], but it should be noticed that the spatial resolution is not crucial for this study as we examine large features of electron precipitation in the ionosphere and the temporal behavior of the hemispherically integrated energy flux. As the technique gives us the electron energy distribution (0.1–100 keV) we can examine the energy flux in different energy ranges.

[14] As we want to study the energy deposition during the entire substorm including both the directly driven growth phase and the loading-unloading substorm event we have looked for isolated substorms proceeded by quiet magnetic conditions and with a good coverage by both PIXIE and UVI. Restricted by the duty cycling of the PIXIE instrument and that the UVI field of view is sometimes too small to cover the entire global substorm we have only found 7 substorms suitable for this study.

Table 1. Onset Times and Geomagnetic Conditions for the Events

Event	Date	Onset	Dst	Kp	AE Max
1	970709	0120	−9	3−	600
2	970709[a]	0400	−17	3−	250
3	970724	1400	12	4−	600
4	970724	1830	8	3−	300
5	970731[a]	0240	−20	4+	1100
6	970828	0245	−6	2+	900
7	970828	0600	−48	4+	500

[a]The stations used to calculate AE_{QL}, AU_{QL}, and AL_{QL} are not well located regarding the regions of intense electron precipitation.

3. Observations

[15] In Table 1 the onset times and geomagnetic conditions for the events are listed. On July 31,1997 there is one isolated substorm and for the other three days there are two subsequent isolated substorms with relatively quiet conditions in between. Although a small negative *Dst* is observed during the two substorms on July 9 both the solar wind speed (370 km/s) and the low solar wind ion pressure (2 nPa) indicate rather steady and quiet solar wind conditions. The positive *Dst* during the two substorms on July 24 may be related to compression pulses caused by abrupt increases in the solar wind ion pressure, from 4 to 8 nPa and from 3 to 6 n Pa, respectively. On July 31 the *Dst* index decreases from 14 to −20 nT during a three hours period, indicating that the substorm occurs in the beginning of a minor magnetic storm, although the ring current energy increase was small as will be shown below. It should also be noticed that the *AE* index peaks at 1100 nT during this event, indicating a rather strong substorm. The two substorms on August 28 occurred when the *Dst* index dropped from −6 to −48 nT and can also be classified as a minor magnetic storm. For these two substorms we also get a substantial increase in the ring current energy as will be shown below. Although the solar wind conditions for the 7 substorms diverse, none of the substorms occur during large magnetic storms.

[16] As we will use geomagnetic indices to derive U_J we should require that the stations used for providing the geomagnetic indices to be well located regarding the regions of intense electron precipitation throughout the substorm. This was not the case for 2 of the substorms as pointed out in Table 1 and will be discussed.

3.1. Electron Energy Fluxes in the Low- and High-Energy Range

[17] In Figures 1 and 2 we show the global maps of total energy flux (0.1–100 keV) and in two different energy ranges (0.1–10 keV and 10–100 keV) for two of the substorms. For this display we have oversampled by a factor of 3 and provided a boxcar averaging. Contamination from the celestial X-ray source, Circinus X-1, entering at slant angles through adjacent pinholes in the PIXIE camera as well as dayglow and contamination from stars in the UV measurements have been removed before deriving the electron distributions from the UV and X-ray emissions. Notice that this is 5 min averages integrated over ~700 km square

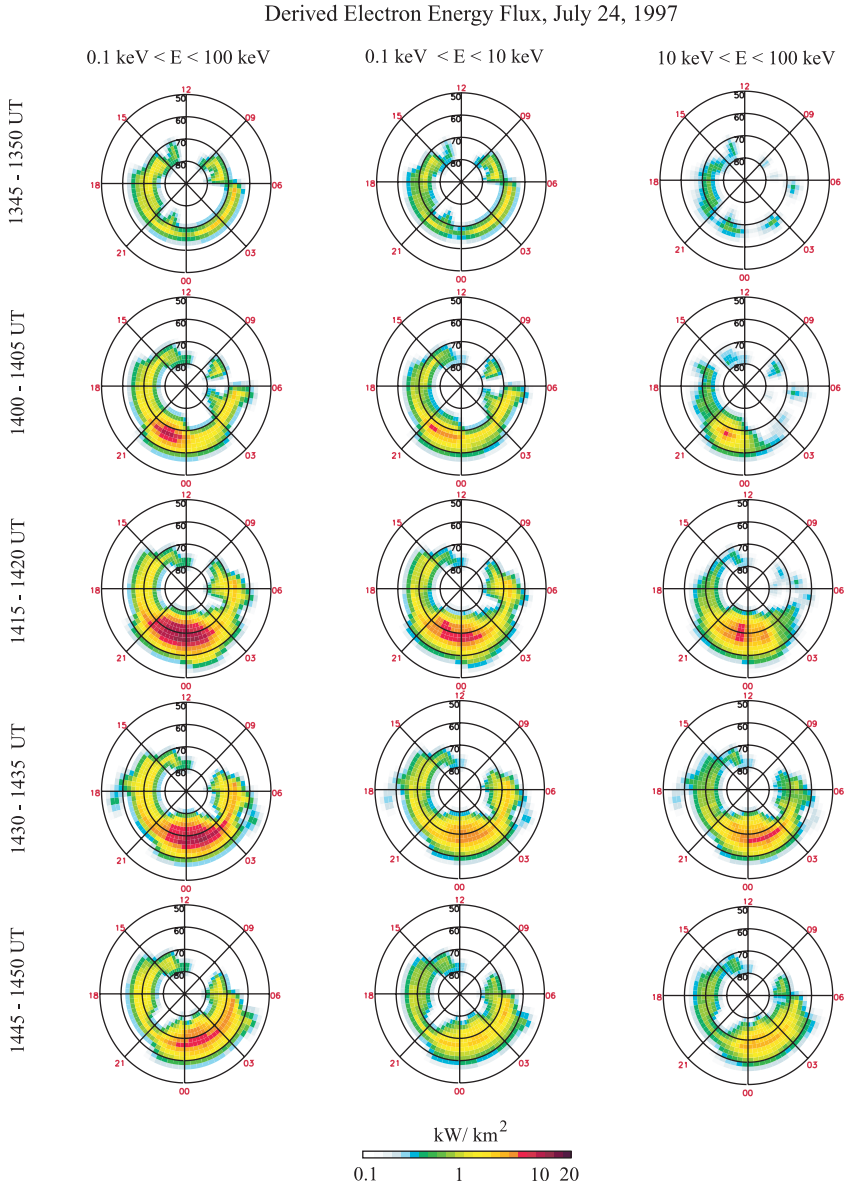

Figure 1. Global maps of electron energy flux derived from UV and X-ray emissions for the July 24 substorm.

boxes, which means that any highly spatially limited or short-lived bursts of precipitation will not be seen.

[18] Figure 1 shows the substorm on July 24 with onset at 1400 UT. Before onset we can see growth phase signatures which are mainly caused by electrons below 10 keV. At onset the energy flux in both energy ranges increases and peaks with almost the same intensity. The energy flux above 10 keV tends to be more confined and peaks at 22 MLT while the energy flux below 10 keV covers a somewhat larger area. The next three time frames show that the amount of energy deposition in the two energy ranges is about the same and that the precipitation area moves toward the dawn. At 1415 UT and 1430 UT a morning maximum at 5–7 MLT is clearly seen in the low-energy range and less significant in the high-energy range (1430 UT).

[19] The substorm on July 31 (Figure 2) which is about twice as strong as the substorm on July 24 has its onset at 0240 UT. Before the onset we see growth phase signatures mainly due to soft electron precipitation below 10 keV. At the onset of the substorm the energy flux in both energy ranges shows a huge increase but the intensity of low-energy electrons seems to be much higher than the intensity of energetic electrons. There seem to be two regions with intense energy flux above 10 keV, peaking at 21 MLT and 23 MLT, while the energy flux below 10 keV is intense in the entire region from 18 MLT to 1 MLT, although there is a slight evidence of the two peaks in this energy range, too. In the next time frame, 0300 UT, soft energy precipitation is significant in the evening around 18 MLT, which does not have its counterpart in the high-energy range. At 0315 UT the soft evening precipitation is much weaker but still present. In both energy ranges the drift of electrons towards dawn is clearly seen. One hour later at 0415 UT the prolonged morning maximum is seen from 5–10 MLT and is the only region of energetic precipitation (>10 keV). Although this substorm is much stronger than the substorm

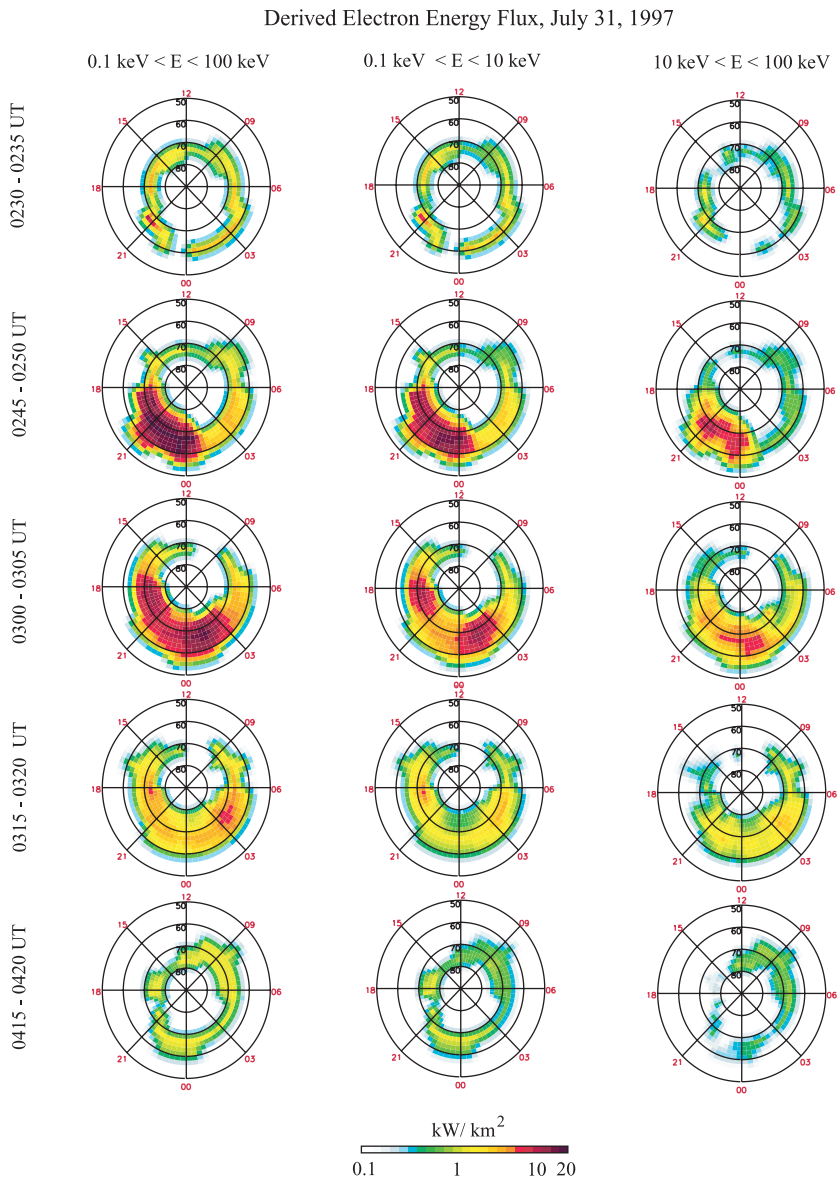

Figure 2. Global maps of electron energy flux derived from UV and X-ray emissions for the July 31 substorm. Notice there is a time gap of 1 hour between the maps from 0315–0320 UT and 0415–0420 UT.

on July 24 it should be noticed that the difference in strength above 10 keV is not as significant as the difference in strength below 10 keV.

3.2. Total Energy Budget for the Substorms

[20] In this section we examine the total energy budget for the substorms by calculating the solar wind energy input due to dayside reconnection, estimated by the ϵ parameter and the U_R, U_J and U_A. We also calculate the solar wind kinetic energy flux onto the cross section of the magnetopause to show the total available energy in the solar wind, U_{SW}.

3.2.1. Solar Wind Energy Input

[21] *Perrault and Akasofu* [1978] and *Akasofu* [1981] showed that the *Dst** index (pressure corrected) can be used to estimate the energy increase of the ring current (U_R, equation (1)).

$$U_R[\mathrm{GW}] = 4 \times 10^4 \left(\frac{\partial Dst^*}{\partial t} + \frac{Dst^*}{\tau} \right) \quad (1)$$

where *Dst** is in nT and τ is the ring current lifetime given in seconds. To estimate the U_J and U_A they used the parameterized relations based on the *AE* index multiplied by 2 to obtain the values for both hemispheres (equations (2) and (3)):

$$U_J[\mathrm{GW}] = 0.1AE \times 2 \quad (2)$$

$$U_A[\mathrm{GW}] = 0.05AE \times 2 \quad (3)$$

For a discussion of the accuracy of their U_A estimate we refer to *Østgaard et al.* [2002]. After comparing these three different forms of energy dissipation ($U_R + U_J + U_A$) with the solar wind input expressed by the solar wind bulk speed, the IMF magnitude and direction they derived the well-known ϵ parameter. [*Akasofu*, 1981].

$$\epsilon = vB^2 \sin^4\left(\frac{\theta_c}{2}\right) l_0^2 \quad (4)$$

Table 2. Hemispherical Joule Heating (U_J) Dependence on *AE*

	a [GW/nT]	*b* [GW]	Stations	HS[a]	*r*[b]	TR[c] [min]	Season
Perrault and Akasofu [1978]	0.05	0.0	–	–	–	–	–
Akasofu [1981]	0.10	0.0	–	–	–	–	–
Ahn et al. [1983]	0.23	0.0	12	N	–	60 (72)	spring
Ahn et al. [1983]	0.19	0.0	71	N	–	60 (72)	spring
Baumjohann and Kamide [1984][d]	0.32	±5.0	12	N	0.74	5 (864)	spring
Baumjohann and Kamide [1984][d]	0.33	±5.0	71	N	0.87	60 (72)	spring
Ahn et al. [1989]	0.33	0.0	12	–	0.90		summer
Richmond [1990]	0.21	1.8	12	–	0.88		winter
Cooper et al. [1995]	0.54	−49.0	12	N	0.62		fall
Cooper et al. [1995]	0.28	−20.0	AMIE	N	0.62		fall
Lu et al. [1995][e]	0.33	−26.0	43	N	0.76		spring
Lu et al. [1998]	0.25	−16.3	68	N	0.91	5 (576)	winter
Lu et al. [1998]	0.20	43.4	68	S[f]	0.76	5 (576)	summer

[a] Hemisphere.
[b] Correlation coefficient of the fit to the data.
[c] Time resolution of the data, in parentheses: number of data points.
[d] Exactly same three days, 17–19 March 1978, as examined by *Ahn et al.* [1983].
[e] This study compares the electromagnetic energy dissipation which is slightly larger than U_{J-NW} but smaller than U_J.
[f] Joule heating is derived for the Southern Hemisphere, but the *AE* index is calculated from 65 and 3 stations in the Northern and Southern Hemisphere, respectively.

where v is the solar wind bulk speed, B is the magnitude of the interplanetary magnetic field, θ_c is the clock angle of the IMF which is defined as the polar angle between the IMF as projected into the y-z plane and the z-axis in GSM coordinates. l_0 is an empirically determined value of the merging region at the subsolar magnetopause assumed to be 7 R_E. The ϵ parameter is frequently used and many studies show that the parameter gives a reasonable estimate of the total energy transferred into the magnetosphere [e.g., *Zwickl et al.*, 1987; *Baker et al.*, 1997; *Lu et al.*, 1998; *Liou et al.*, 1998], although some studies find that the viscous interaction between the solar wind and the magnetosphere must account for some energy transfer in order to balance the total energy budget [*Lu et al.*, 1998; *Knipp et al.*, 1998]. Efforts have been made to find other energy transfer parameters that give better correlation with auroral measurements [see, e.g., *Gonzalez et al.*, 1994; *Liou et al.*, 1998] but without providing a more accurate estimate of the magnitude of the energy transfer.

3.2.2. Ring Current

[22] To estimate the ring current energy injection rate U_R we use equation (1). However, there is no unambiguous way to choose either the scaling factor (i.e., 4×10^4 as used by *Akasofu* [1981]), the ring current life time τ or how to obtain the pressure corrected *Dst**. Different studies suggest different values and a brief discussion is therefore needed.

[23] The scaling factor a was set to 4×10^4 by *Akasofu* [1981] which was adopted in the study by *Baker et al.* [1997] and *Lu et al.* [1998]. *Prigancova and Feldstein* [1992] used a slightly lower value $a = 2.7 \times 10^4$. We adopt the former value and keep in mind that we might get a slight overestimate. Variations in the solar wind pressure will modulate currents flowing on the dayside magnetopause [*Gonzalez et al.*, 1994] and lead to a compression of the magnetosphere that will be observed as an increase in the *Dst* index. To remove this effect as it is not related to the ring current we calculate the pressure corrected *Dst**.

$$Dst^*[nT] = Dst - \Delta H \tag{5}$$

The pressure correction term ΔH used by *Akasofu* [1981] adopted from *Siscoe et al.* [1968] is

$$\Delta H[nT] = 1.31 \times 10^5 \left(p_2^{1/2} - p_1^{1/2}\right) \tag{6}$$

where p is the solar wind dynamic pressure. However, it seems that a more updated correction is given by *Gonzalez et al.* [1994, and references therein]

$$\Delta H[nT] = 0.2 \frac{nT}{(eV\ cm^{-3})^{1/2}} p^{1/2} - 20nT \tag{7}$$

which in SI units becomes

$$\Delta H[nT] = 5 \times 10^5 \frac{nT}{(Jm^{-3})^{1/2}} p^{1/2} - 20nT \tag{8}$$

[24] The ring current life time which depends on loss processes mainly due to charge exchange between ring current ions and exospheric neutrals is not thought to be constant. *Akasofu* [1981] suggested that τ = 20 hr for $\epsilon <$ 500 GW and τ = 1 hr for $\epsilon \geq$ 500 GW while both *Prigancova and Feldstein* [1992] and *Gonzalez et al.* [1994] suggest more differentiated τ values for different magnetic conditions. In the study by *Lu et al.* [1998] a reasonable compromise between the various results has been made and we adopt the values from that study.

[25] To summarize, we use equation (8) for the pressure correction [*Prigancova and Feldstein*, 1992; *Gonzalez et al.*, 1994], and equation (1) to estimate U_R, with $a = 4 \times 10^4$ and τ = 4, 8 or 20 hours for *Dst** <−50, <−30 and >−30 nT, respectively [*Lu et al.*, 1998].

3.2.3. Joule Heating

[26] To estimate the Joule heating rate from the AE index there are different results that may be applied. They are all on the form:

$$U_J[\mathrm{GW}] = aAE + b \tag{9}$$

and different studies have arrived at different a and b values as listed in Table 2.

[27] To decide which of these values (a and b) to use we consider the following. As we use the quick look AE index we should choose values of a and b that are derived from a similar number of stations, as the AE_{68} on average is 35% higher than AE_{12} [*Lu et al.*, 1998], a tendency that also can be seen in the work of *Tsurutani et al.* [1985]. This implies that the scaling factor a obtained when a large number of stations are used should be smaller than when only ≤ 10 stations are used. This leads us to believe there is some inconsistency in the a value derived by *Baumjohann and Kamide* [1984] as using AE_{12} or AE_{71} does not seem to affect their result significantly. In fact they get a higher a value when AE_{71} are used, contrary to what one would expect. Examining exactly the same days *Ahn et al.* [1983] get a ~20% difference in the a value by using different numbers of stations. The a value found by *Cooper et al.* [1995] based on AE_{12} during a severe magnetic storm is twice as big as the a value found in the others studies. This large value is mainly due to the very large polar potential gradients they derive from the AMIE procedure which gives a large U_J. The authors also point out, that during such strong magnetic activity, the current systems will move equatorward of the 12 stations that are used to derive the standard AE index and hence the AE_{12} will not fully reflect the ionospheric currents. They also estimated an AE index from the predicted magnetic disturbances resulting from the currents obtained by the AMIE procedure, which is 50% larger than the AE_{12} index (their Figure 5). For the U_J (AE_{AMIE}) any bias introduced by a too large AMIE estimated electric field will then be somewhat cancelled out and the a value becomes closer to what other studies have found. Consequently, we think $a = 0.28$ rather than $a = 0.54$ represents their best estimate. The a value obtained by *Lu et al.* [1998], using AE_{68} and U_J from the AMIE procedure obtained values close to the ones from *Ahn et al.* [1983]. In another paper, *Ahn et al.* [1989] derived the conductivity from X-ray imaging data and arrived at $a = 0.33$ with a high correlation coefficient ($r = 0.90$). *Richmond* [1990] used AE_{12} and the AMIE procedure to calculate the U_J and found $a = 0.21$ with a high correlation coefficient ($r = 0.88$). *Lu et al.* [1995] found a a value of 0.33. This value is for the electromagnetic energy dissipation, which they found to be slightly larger than the neutral wind corrected Joule heating, U_{J-NW}, which was found to be ~83% of the U_J that is usually calculated (i.e., with neutral wind effects included). Even if they used 43 stations to estimate the AE index, they emphasize that there was a big data gap over the Russian area, which may explain the large a value they obtained.

[28] To summarize this brief discussion all the values found by *Ahn et al.* [1983, 1989] and *Richmond* [1990] based on AE_{12} seem to be equally good as they all give high correlation coefficients. However, we notice that the values have a weak seasonal dependence. Disregarding the AE_{12} results from *Baumjohann and Kamide* [1984] and *Cooper et al.* [1995], for reasons mentioned above, we only have one a value (using AE_{12}) for each season; $a = 0.33$ for summer [*Ahn et al.*, 1989], $a = 0.21$ for winter [*Richmond*, 1990] and $a = 0.23$ for equinox [*Ahn et al.*, 1983]. These values may reflect the seasonal dependence that arises from the solar UV conductance leading to larger U_J in the summer hemisphere. This seasonal effect has been theoretically estimated by *Nisbet* [1982]. As his estimate is given as a function of both AL and AU, we find by making a rough assumption of $AL = 3AU$ that $U_J = 0.32AE - 40.0$ for summer and $U_J = 0.07AE + 2.9$ for winter. In this study where the events are from solstice we add the values obtained by *Ahn et al.* [1989] (summer) and *Richmond* [1990] (winter), i.e., $a = 0.33 + 0.21$ and $b = 0.0 + 1.8$ to get the Joule heating in both hemispheres (equation (10)).

$$U_J[\mathrm{GW}] = 0.54AE + 1.8 \tag{10}$$

This implies a seasonal difference of ~50%, which is larger than the 12% difference *Emery et al.* [1999] found for the 10 day severe magnetic storm period, November 1993, and may be an indication of a smaller seasonal difference during strong magnetic activity. On the other hand the small seasonal difference they found may partly be explained by an underestimate of the conductance in the summer (southern) hemisphere as fewer magnetometer stations were used to estimate the energy deposition by precipitation in the Southern Hemisphere than in the Northern Hemisphere. Another indication that the seasonal effect is dependent on the magnetic activity can be interpreted from the linear relations between U_J and AE for the two hemispheres found by *Lu et al.* [1998]. For small AE values their U_J is significantly higher in the summer hemisphere, but tend to be similar in the two hemispheres for large AE values. We should also point out that there are at least two other factors that may lead to errors in the U_J estimate. *Lu et al.* [1995] and *Emery et al.* [1999] found that the U_J should be decreased by 10–30% if a compete calculation of U_J is carried out including the neutral wind mechanical energy increase U_{NW}. As the neutral winds are more tightly coupled to the ion drifts in the summer hemisphere due to the higher electron density, *Emery et al.* [1999] found that the neutral wind corrected Joule heating, U_{J-NW}, in the summer hemisphere could be smaller than U_{J-NW} in the winter hemisphere. *Codrescu et al.* [1995] and *Lu et al.* [1998] found that taking into account realistic electric field variability, the U_J estimate could be increased by 10–30%. We should emphasize that the U_J estimates used in this study include U_{NW} and disregard the electric field variability. As these two effects are in the same range and opposite they may cancel, but these considerations also indicate that the U_J value we use is somewhat uncertain. For intense magnetic storms, like the one studied by *Cooper et al.* [1995] where the *Dst* index reached beyond −300 nT, the currents would probably move equatorward of the stations and in such a case our U_J (AE_{QL}) (equation (10)) would probably provide an underestimate.

3.2.4. Auroral Electron Energy Deposition in Both Hemispheres

[29] We calculate the U_A in both hemispheres by simply multiplying the U_A obtained from UV and X-ray emissions in the Northern Hemisphere by 2. This is consistent with the study by *Lu et al.* [1998] who estimated the U_A in both hemispheres by using the AMIE procedure. Although the absolute values of their estimates may be uncertain (as discussed by *Østgaard et al.* [2002]) the energy deposition

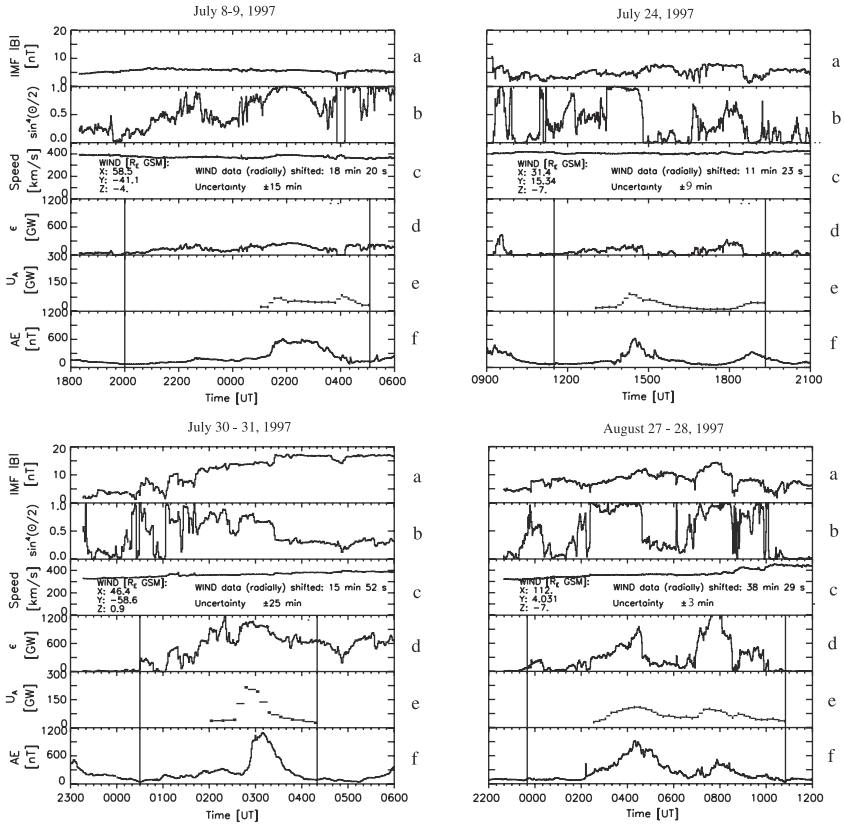

Figure 3. Solar wind energy input measured by Wind, ionospheric energy deposition derived from PIXIE and UVI and *AE* index from Kyoto for all the events. (a) The scalar interplanetary field magnetic field. (b) $\sin^4\left(\frac{\theta_c}{2}\right)$, where θ_c is the clock angle of the interplanetary field. (c) The solar wind bulk speed. (d) Estimate of the solar wind energy transfer into the magnetosphere based on the semiempirical ϵ parameter. (e) The global energy deposition by electron precipitation in the northern ionosphere derived from UV- and X-ray emissions. (f) The *AE* quick look index from Kyoto. The vertical lines indicate the beginning of the growth phase and the end of the image data. The Wind data are shifted due to the radially distance of the spacecraft and the expected ~5 min propagation time from the subsolar point to the ionosphere [*Kan et al.*, 1991].

rate in the two hemispheres are almost similar for the entire event they examine.

3.2.5. Solar Wind Kinetic Energy Flux

[30] Even though most of the energy transfer from the solar wind to the magnetosphere is thought to be due to dayside reconnection approximated by the ϵ parameter there may be other energy transfer mechanisms as well. We have therefore calculated the solar wind kinetic energy flux onto the cross section of the magnetopause

$$U_{SW} = 1/2\rho v^3 A \tag{11}$$

where ρ is the solar wind mass density (including the Helium content in the solar wind), v is the solar wind radial speed and A is the magnetopause cross section. To estimate A we have used the results from *Shue et al.* [1997] who found that A depends on the solar wind dynamic pressure and the IMF B_Z value. The over all coupling efficiency of the solar wind kinetic power to the magnetosphere is thought to be ~1% [*Stern*, 1984] although others [*Lu et al.*, 1998] suggest as much as 4%. We calculate the solar wind kinetic energy flux just to show the total available energy in the solar wind and treat the fraction of energy transfer due to another transfer mechanism than dayside reconnection (e.g., viscous interaction) as a free parameter and use our data set to make an estimate of this fraction.

3.2.6. Total Budget

[31] In Figure 3 we show the solar wind data measured by Wind, the ionospheric energy deposition derived from PIXIE and UVI and the *AE* quick look index from Kyoto for all the events. In the upper three panels (a, b, and c) we have plotted the interplanetary field strength ($|B|$), solar wind bulk speed (v) and $\sin^4\left(\frac{\theta_c}{2}\right)$ in GSM coordinates. These three parameters are needed to estimate the ϵ parameter (equation (4)) which is plotted in panel d. The original data is transferred from the original 79 s and 46 s time resolution to a 1 min resolution for both data sets. The solar wind data is shifted in time due to the radially distance of the Wind spacecraft relative to the subsolar point of the magnetopause. We have also added 5 min to account for the propagation time for a disturbance in the solar wind to affect the inner magnetosphere and thereby be observable in the ionosphere and on the ground [*Kan et al.*, 1991]. To estimate the uncertainty of the time shift we have used the results from *Collier et al.* [1998] who showed that the uncertainty is proportional to the $d_\perp/d_\parallel$, where $d_\perp$ is the distance from the

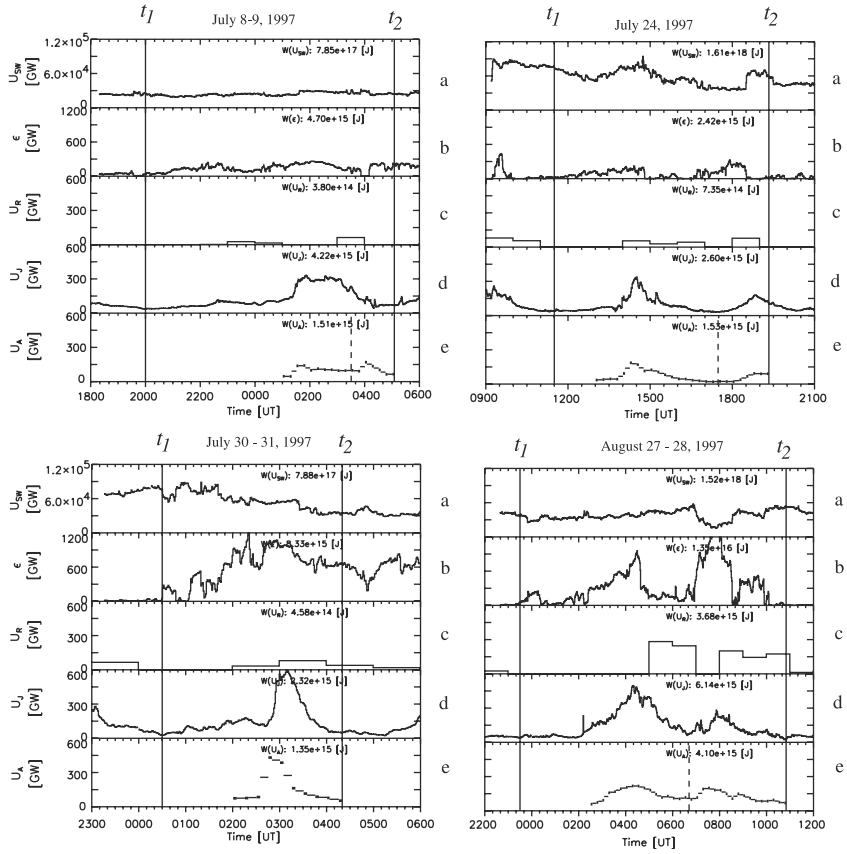

Figure 4. The energy transferred from the solar wind and the various energy dissipations into the ionosphere. (a) The available solar wind kinetic energy flux onto the magnetopause cross section (U_{SW}). (b) ϵ parameter. (c) The energy increase of the ring current (U_R). (d) The Joule heating of the ionosphere in both hemispheres (U_J). (e) The global energy deposition by electron precipitation in both hemispheres derived from UV- and X-ray emissions (U_A). The solid vertical lines denote the time interval used for integration from t_1 to t_2. The dotted vertical lines denote the separation between two substorms. The time-integrated energy dissipation (e.g., $W(U_{SW})$) is calculated in each panel.

Earth-Sun line (Wind location $= \sqrt{Y^2 + Z^2}$) and $d_{\|}$ is the distance upstream from the magnetopause (WIND location = $X - 10\mathrm{R_E}$). The location of the Wind spacecraft, the time shift and the uncertainty of this time shift is indicated in Panel c for each event. In Panel e we show the U_A (0.1–100 keV) derived from UV and X-ray emissions. Between the 5 min averages (thick lines) we have performed a linear interpolation and plotted that value as a constant value in the intermediate 10 min interval (thin lines). In the bottom panel we show the 1 min quick look *AE* index. As we want to time-integrate the energy transfer into the magnetosphere prior to and during the substorms we have to consider carefully when to start the integration. For this purpose we examine the *AE* index and determine the quietmost time before the substorm. This time is taken to be the beginning of the growth phase and is indicated as vertical lines. For all the events this time seems to correspond fairly well with the increase in the ϵ parameter, indicating that the time shifts of the solar wind data are reasonable.

[32] In Figure 4 we show the different forms of energy in the solar wind-magnetosphere-ionosphere system during the substorms. Panel a shows the available solar wind kinetic energy flux onto the magnetopause cross section (U_{SW}) and panel b shows the energy transfer estimated by the ϵ parameter. The next three panels shows the U_R, U_J and U_A. For the different forms of energy we have calculated the time-integrated value $W(U_X)$ from t_1 to t_2.

$$W(U_X)[J] = \int_{t_1}^{t_2} U_X(t)dt \tag{12}$$

4. Discussion

4.1. Electron Energy Fluxes in the Low- and High-Energy Range

[33] To examine the differences in the low- and high-energy ranges of energy fluxes we show (Figure 5) the time development of the hemispherically integrated electron energy flux. Solid, dotted and dashed lines are the energy flux from 0.1 keV to 100 keV, 0.1–10 keV and 10–100 keV, respectively. For all the events the energy flux above and below 10 keV is fairly similar, except for the July 31 substorm. For this very strong event we can see that the electrons below 10 keV contribute about twice as much to the total energy flux compared to the electrons above 10 keV. In Table 3 we have listed the peak values during expansion phase, as well as the increase ratio from growth

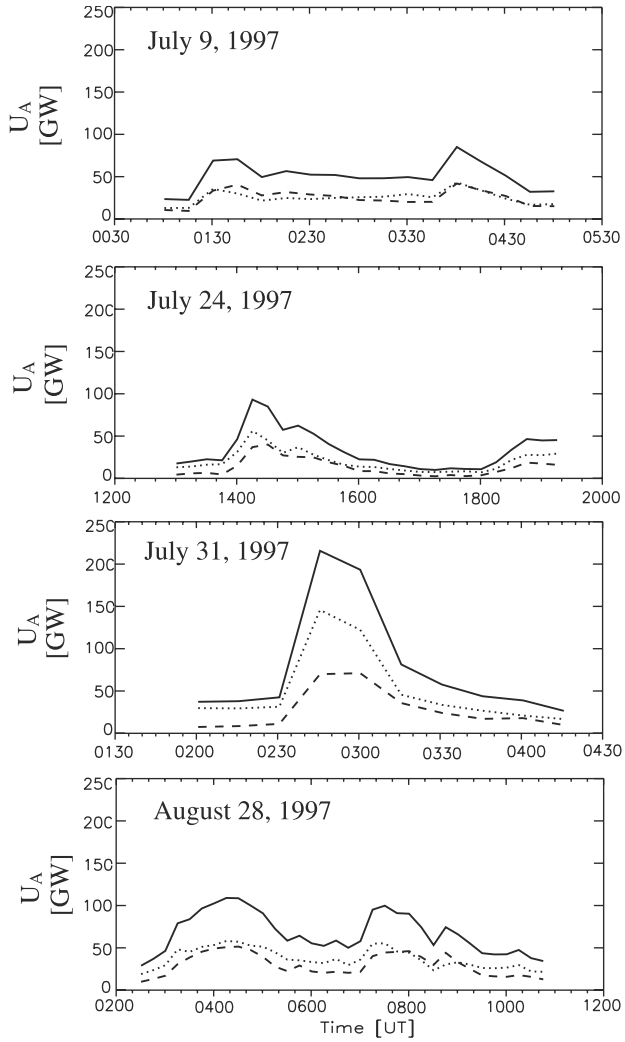

Figure 5. The electron energy flux for the four days. Solid line: Total energy flux (0.1–100 keV). Dotted line: Energy flux from low-energy electrons (0.1–10 keV). Dashed line: Energy flux from high-energy electrons (10–100 keV).

phase to expansion phase in the two energy ranges for 6 of the substorms. The second substorm on July 24 is not included because the duty cycling of the PIXIE instrument prevents us from deriving energy spectra in the high-energy range for that entire substorm. For electrons below 10 keV the energy flux for the July 31 substorm peaks at 145.8 GW (67% of total energy), about 3–4 times more than during the more moderate substorms which peak from 35.5 GW to 58.1 GW (47–58% of the total energy). However, looking only at electrons above 10 keV, the energy flux peaks at 71.1 GW which is only slightly higher than the other substorms varying from 40.0 GW to 51.4 GW. These results indicate that the soft electrons define the maximum intensity of the substorm.

[34] The ratios of increase from growth phase to expansion phase listed in the two rightmost columns show that the electrons above 10 keV tend to have a greater intensification than the electrons below 10 keV at substorm onset. We also noticed earlier that the energetic electrons seem to be more confined azimuthally (Figures 1 and 2). This can partly be explained by the fact that the growth phase is dominated by soft precipitation and the electron energy flux below 10 keV is already at some intensity before substorm onset. It may also indicate that the energetic electrons play a key role in the triggering of the substorm onset where the energetic precipitation starts out in a narrow flux tube.

[35] We also want to make some comments on the different locations and durations of the morning maximum for the two substorms shown in Figures 1 and 2. The morning maximum on July 24 never gets further than 7 MLT and only lasts for 30 minutes but on July 31 it reaches beyond 11 MLT and stays for more than 1 and a half hours. On July 31 the energy input to the magnetosphere as well as the energy deposition into the ionosphere is high and the flux of injected quasi-trapped energetic particles is probably high. This implies that wave-particle interaction, which is the most probable mechanism for the morning maximum can last as long as the flux level is high enough [*Østgaard et al.* 2000, and references therein]. For the July 24 event, the flux of injected quasi-trapped particles is probably much lower and soon decreases below the threshold level for the wave-particle interaction to occur. The difference in duration may also explain the difference in location as the morning maximum needs time to extend to the dayside. The convective electric field as indirectly seen from the difference in the ϵ parameter for the two events, is much larger during the July 31 and will tend to move the morning maximum onto the dayside. This interpretation implies that we have eastward movement on two different time scales and during two different phases of the substorm. First the rapid eastward movement from the onset region in the midnight sector during the expansion phase of the substorm which can be explained by gradient and curvature drift of the electrons [*Østgaard et al.*, 2000]. Then the slow movement towards dawn of the prolonged morning maximum, which is thought to be caused by wave-particle interaction [*Østgaard et al.*, 2000] during the recovery phase of the substorm. This slow movement may be related to an expansion of the wave-particle interaction region where the convective electric field may play an important role.

[36] We have also calculated how much of the U_A derived from UVI and PIXIE we would estimate if only the UVI is used. In other words, how much of U_A is due to the hard tail in the electron spectrum we derive from the X rays. By only

Table 3. Comparison of Energy Flux by Auroral Electrons in the Low- and High-Energy Range

		EP[a] [GW] (%)[c]		EP/GP[b] [Ratio]	
Event	Date	Low	High	Low	High
1	970709	35.5 (47)	40.6	2.8	4.3
2	970709	43.2 (51)	41.9	1.7	2.1
3	970724	56.2 (58)	40.0	3.3	8.7
4	970724	–	–	–	–
5	970731	145.8 (67)	71.1	4.9	9.5
6	970828	58.1 (53)	51.4	3.1	5.2
7	970828	55.4 (55)	46.1	1.9	2.2

[a] EP: Expansion phase of the substorm.
[b] GP: Growth phase of the substorm.
[c] In parentheses is the percentage of energy flux below 10 keV relative to the total (0.1–100 keV).

Table 4. Total Energy Budget for the Substorms

Date (hours)[e]	Number[a]	$W(U_R)$ [10^{14}J] (%)[f]	$W(U_J)$[b] [10^{14}J] (%)[f]	$W(U_A)$[b] [10^{14}J] (%)[f]	$W(U_T)$[c] [10^{14}J]	$W(\epsilon)$ [10^{14}J]	$W(U_{SW})$ [10^{16}J]	CE[d] [%]
970709 (8.5–4)	2	3.8 (6)	42.2 (69)	15.1 (25)	61.1	47.0	78.5	0.8
970724 (7.8–6.3)	2	7.4 (15)	26.0 (53)	15.3 (32)	48.7	24.2	161.0	0.3
970731 (3.7–2.3)	1	4.6 (11)	23.2 (56)	13.5 (33)	41.3	83.3	78.8	0.5
970828 (10.8–8.3)	2	36.8 (26)	61.4 (44)	41.0 (30)	139.2	135.0	152.0	0.8
Average		(15)	(56)	(29)				

[a]Number of substorms.
[b]Both hemispheres.
[c]$W(U_T) = W(U_R) + W(U_J) + W(U_A)$.
[d]CE: Coupling Efficiency defined as $W(U_T)/W(U_{SW})$.
[e]Hours of integration for: $W(U_R)$, $W(U_J)$, $W(\epsilon)$—and: $W(U_A)$.
[f]Percent of $W(U_T)$.

using UVI, assuming that the LBHL is a measure of the total electron energy flux we will estimate about 90–100% during growth phase and expansion phase and closer to 80% during recovery phase. Comparing the electron energy flux derived at different local times we get between 90–100% in the day, dusk and midnight sector and closer to 80% in the dawn sector. These results are consistent with the existence of hard electron spectra in the postmidnight to dawn sector during the recovery phase of substorms. Although we find that U_A would have been slightly underestimated by using only UVI the error is in the same range as the uncertainties of U_R and U_J. The energy contribution from the hard tail in the electron spectrum is at most 20–30% on a global scale, but for physical processes like Hall conductance increases, cosmic radio wave absorption or wave-particle interaction this tail is the most important part of the energy spectrum. We should also point out that emission lines in the LBH band are produced by both electron and proton precipitation [see, e.g., *Frey et al.*, 2001], while the X rays measured by PIXIE are produced by electrons only. The ions below ~30 keV are found to contribute about 15% of the total energy deposition by particle precipitation during moderate magnetic activity [*Galand et al.*, 2001].

4.2. Total Energy Budget for the Substorms

[37] In Table 4 we have listed the time-integrated energy depositions and energy transfer from the solar wind (as shown in Figure 4). For $W(U_R)$, $W(U_J)$ and $W(U_A)$ we have calculated the fraction (in %) of the total energy dissipation ($W(U_T) = W(U_R) + W(U_J) + W(U_A)$). Notice that the time of integration is shorter for $W(U_A)$ than for the other energies due to the limited operation time of the imagers on Polar (see Table 4). For the days with more than one substorm we have also calculated the $W(U_A)$ for each single substorm (not listed in Table 4). The times for separating between two substorms on the same day are shown by dashed lines in Figure 4, panel e. The intensity of the substorms varies from 6.6–24.0 × 10^{14} J, with a mean of 13.5 × 10^{14} J, which is an order of magnitude larger than suggested by *Akasofu* [1981] (1.4 10^{14} J). Part of this may be that our substorms are more intense than the substorms *Akasofu* [1981] examined, but maybe more important; the parameterized method he used to estimate U_A only gives 1/3 of the U_A [*Østgaard et al.*, 2002]. We find that on average $W(U_A)$ is ~29% of the total energy dissipation, $W(U_T)$, which may be a lower estimate as the integration times used for $W(U_A)$ are shorter than for the other energies (see Table 4).

[38] $W(U_R)$ is small except for the two substorms occurring on August 28 during a minor magnetic storm. For these two substorms the $W(U_R)$ is as much as 26% of the $W(U_T)$, but the average of 15% is still similar to the substorms on July 24 where the $W(U_R)$ is fairly small. Remember that the U_R might have been overestimated by using the scaling factor (4 × 10^4) [*Akasofu*, 1981; *Baker et al.*, 1997; *Lu et al.*, 1998] compared to the more conservative value (2.7 × 10^4) suggested by *Prigancova and Feldstein* [1992].

[39] The average value found for $W(U_J)$ is 56% which may be a lower estimate as the stations used to calculate the *AE* index were not well located for the substorms occurring on July 31 and July 9 (second substorm). Another source of underestimate is that during strong events (*AE* > 1000 nT) as the one on July 31, the electrojets may move southward of the stations and will be poorly detected.

[40] We find the ratio of $W(U_J)$ to $W(U_A)$ to be ~2, which is similar to what *Lu et al.* [1998] found as an average value of U_J/U_A for the two hemispheres. The results from *Lu et al.* [1998] also imply that U_J/U_A is larger in the Southern Hemisphere (~3) than in the Northern Hemisphere (~2) which may reflect the increase of U_J due to sunlit conditions. This is similar to what we found in the discussion of U_J as a function of *AE* for winter and summer conditions (section 3.2.3). The slight difference in U_A in the two hemispheres that can be seen from *Lu et al.* [1998] may be explained by the fact that UVI global images were used to derive U_A in the Northern Hemisphere, while mostly DMSP and NOAA data were used to derive U_A in the Southern Hemisphere. *Akasofu* [1981] also found the ratio $W(U_J)/W(U_A)$ to be ~2, although he underestimated both values by a factor of ~3. *Ahn et al.* [1983] found that the average value of the ratio U_J/U_A is 4, as he underestimated U_A by a factor of ~3 [*Østgaard et al.*, 2002] and used a conservative value for U_J. *Prigancova and Feldstein* [1992], who found a ratio of 1.3, underestimated the U_A by using the results from *Spiro et al.* [1982] which only provides 50–75% of the U_A [*Østgaard et al.*, 2002] (both hemispheres), but this underestimate seems to be cancelled by estimating the U_J based on only one hemisphere. *Richmond* [1990] found the ratio to be ~3, but they probably underestimated the U_A by ~30% [*Østgaard et al.*, 2002]. For the most active day of the magnetic storm, *Emery et al.* [1999] found the ratio to be 3.2 (2.6) in the summer (winter) hemisphere and *Knipp et al.* [1998] found the average ratio U_J/U_A of the entire storm period to be 2.6. As already pointed out, the U_A values used by *Knipp et al.* [1998] and *Emery et al.* [1999] might have been under-

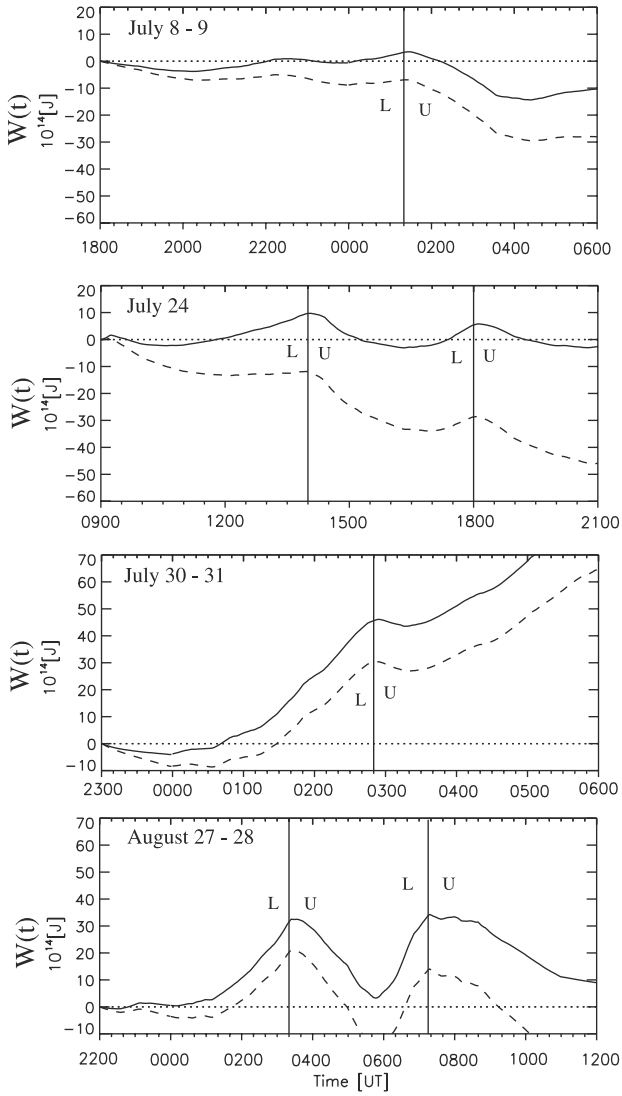

Figure 6. The time-integrated total energy balance between energy input and output ($W(t)$) as a function of time, see equation (13). Dashed line: Energy input estimated as ϵ only. Solid line: Energy input is calculated as ϵ + 0.0017 U_{SW}, where U_{SW} is the kinetic solar wind flux given by equation (11). We have indicated the times of energy loading (L) and energy unloading (U).

estimated in the summer hemisphere. *Lu et al.* [1995] found the ratio to be ~4, which may be due to an underestimate of the U_A, due the data gap over the Russian area.

[41] As seen from Table 4, the time-integrated total energy dissipation ($W(U_T)$) is distributed as 15%, 56% and 29% to $W(U_R)$, $W(U_J)$ and $W(U_A)$, respectively, which is very close to what *Knipp et al.* [1998] found for the entire 10 days of the magnetic storm period of November, 1993 (17%, 60%, 23%). The main difference seems to be that our U_A is larger than in their study. In the rightmost column of Table 4 we have listed the coupling efficiency, expressed by the ratio $W(U_T)/W(U_{SW})$. The coupling efficiency is from 0.3–0.8%, which is in reasonable agreement with the 1% that according to *Stern* [1984] is the widely cited order of magnitude of the energy extracted from the solar wind. The higher coupling efficiency found by *Knipp et al.* [1998] (6.9%) and *Lu et al.* [1995] (1.5%) can be explained by the different estimates of the magnetospheric cross section they used. We use the cross section suggested by *Shue et al.* [1997], which depends on the solar wind pressure and IMF B_Z and is usually $\pi \times 10^2$ R_E^2. *Knipp et al.* [1998] have used $7^2 R_E^2$ and *Lu et al.* [1995] have used 15^2 R_E^2. Using the same cross section as we do, their coupling efficiencies would both become 1.1%. We should point out that *Lu et al.* [1995] have not considered energy increase of the ring current, so their coupling efficiency should be slightly increased. *Lu et al.* [1998], which used the same cross section that we do [*Shue et al.*, 1997] obtained a coupling efficiency as high as 3.6%. However, their average value of U_{SW} (11,000 GW) is not in agreement with their Figure 4, where the average U_{SW} seem to be closer to 20,000 GW.

[42] Comparing $W(\epsilon)$ and $W(U_T)$ we see that the ϵ parameter does not always provide enough energy to balance the U_T, similar to what *Knipp et al.* [1998] found, but contrary to what *Akasofu* [1981], *Stern* [1984], *Gonzalez et al.* [1994], *Baker et al.* [1997], and *Lu et al.* [1998] have reported. The main reason for this difference is that the U_A (and U_J) estimated in their studies is 2–4 times smaller than shown in the present study. For the July 24 events the $W(U_T)$ is twice as much as the $W(\epsilon)$. One might argue that the magnetosphere stores energy from the solar wind and the two values should not necessarily balance, but for the July 24 events it should be noticed that the energy transfer estimated by ϵ during the two substorms is remarkably low, while the $W(U_{SW})$ is large and the $W(U_T)$ is in the same range as the other substorms (Table 4 and Figure 4). Even integration of the ϵ parameter from an earlier time does not alter this, because another substorm at 0800–1100 UT probably dissipated most of the solar wind energy transferred before and during that event.

[43] In Figure 6 we have plotted the time-integrated total energy balance between energy input and output as a function of time

$$W(t) = \int_{t_1}^{t} \epsilon(t) - U_T(t)dt \qquad (13)$$

As can be seen from the two upper panels and the bottom panel the ϵ parameter (dashed line) does not provide enough energy to balance U_T. The overall negative slope of $W(t)$ is nonphysical as the system cannot dissipate more energy than is transferred into it. This indicates that there has to be some other energy transfer mechanism than dayside reconnection or that the merging area, l_0^2, in the ϵ function (see, equation (4)) should be increased. We find that adding 0.17% of the U_{SW} to the ϵ term is needed to balance the energy budget. This is shown by the solid line. For the July 24 events this additional term (0.17% of the U_{SW}) contributes with similar amount of energy as the $W(\epsilon)$ but only 10–20% of $W(\epsilon)$ for the other events. In Figure 6, increasing $W(t)$ (solid line) indicates the loading of energy (L) during substorm growth phase and decreasing $W(t)$ indicates the energy dissipation (U, for unloading) from substorm onset through the expansion phase.

[44] An energy transfer mechanism due to viscous interaction was first suggested by *Axford and Hines* [1961], but as the physical meaning of viscous interaction in a collisionless plasma is not obvious [*Parks*, 1991] some kind of wave-particle interaction has been suggested to be the coupling mechanism. In a recent paper by *Farrugia et al.* [2001], Kelvin-Helmholtz instability has been considered to be a major contributor to viscous coupling, although their results only apply to northward IMF conditions. Efforts have been made to quantify the energy transfer efficiency by such a mechanism. By calculating the U_T during 11 intense northward IMF events that lasted for several hours, where the merging of field lines is almost negligible and hence the ϵ would be close to zero, *Tsurutani and Gonzalez* [1995] found that 0.1–0.4% of the U_{SW} was needed to balance the energy budget. It should be noticed that this study used the very conservative values from *Akasofu* [1981] to estimate the U_J and U_A, which means that their energy transfer efficiency should be closer to 0.3–1.2% of the U_{SW} rather than 0.1–0.4%. Our finding of a 0.17% energy transfer efficiency in addition to the ϵ provides more support to such an interpretation.

[45] For the July 31 event there is more energy transferred into the magnetosphere than dissipated during the substorm, indicating that there are energy sinks we have not considered. Such energy sinks might be the plasma sheet heating or the ejection of plasmoids down the tail. For the magnetic cloud event *Lu et al.* [1998] estimated the plasma sheet heating to be 100 GW and in the same range as the energy dissipated by electron precipitation. In a statistical study on plasmoids *Ieda et al.* [1998] have estimated the energy released tailward by plasmoids in the course of a substorm to be roughly 10^{15} J. However, for the July 31 event the excess of energy is as much as 42×10^{14} J ($W(\epsilon) - W(U_T)$, see Table 4) when only the $W(\epsilon)$ energy transfer term is considered (i.e., if $W(U_{VI})$ is set to zero). As the plasma sheet heating and the release of energy by plasmoids may not account for more than half of this energy excess, it is likely that there is a net energy gain in the magnetosphere during this event.

5. Conclusion

[46] Based on electron energy distributions derived from UV and X-ray emissions we have studied the hemispherically integrated energy flux by electron precipitation (U_A) for 7 substorms. Our main findings are:

1. The electrons below 10 keV dominate the total energy flux during growth phase and the intensity of soft electron precipitation seems to define the maximum intensity of the substorm.

2. Electrons above 10 keV show a greater intensification at substorm onset and are more confined azimuthally during the expansion phase.

3. By only using UV emissions to derive the electron energy flux, one would get 80–100% of the U_A depending on the substorm phase and the magnetic local times that are estimated.

4. Our estimate of U_A is a factor 2–4 larger than reported in most of the earlier studies [see *Østgaard et al.*, 2002].

By using the most appropriate parameterized methods to estimate the energy increase of the ring current (U_R) and the Joule heating in both hemispheres (U_J) we have estimated the total energy dissipation rate during substorms ($U_T = U_R + U_J + U_A$) and found that:

5. The contributions to the total time-integrated energy dissipation over the duration of the substorm, $W(U_T)$, from $W(U_R)$, $W(U_J)$ and $W(U_A)$ on average are 15%, 56% and 29% of $W(U_T)$.

6. For some events the ϵ parameter does not provide enough energy transfer into the magnetosphere to balance U_T. An additional energy transfer mechanism is needed to balance the energy budget. We find that a viscous interaction that transfer 0.17% of the U_{SW} into the magnetosphere is sufficient to balance the total energy dissipation U_T, which is on the low side of the viscous interaction efficiency found by *Tsurutani and Gonzalez* [1995].

[47] **Acknowledgments.** This study was supported by the Norwegian Research Council (NFR) and by the National Aeronautic and Space Administration (NASA) under contract NAS5-30372 at the Lockheed–Martin Advanced Technology Center, the University of Washington contract 832213 to the University of Alabama in Huntsville and NASA grant NAG5-6986 to the University of Alabama in Huntsville. We acknowledge the World Data Center for Geomagnetism (T. Kamei), Kyoto, Japan for providing the preliminary Quick look AE, AL and AU indices.

[48] Janet G. Luhmann thanks Barbara Emery and another referee for their assistance in evaluating this paper.

References

Ahn, B. H., S.-I. Akasofu, and Y. Kamide, The Joule heat production rate and the particle energy injection rate as a function of the geomagnetic indices *AE* and *AL*, *J. Geophys. Res.*, *88*, 6275–6287, 1983.

Ahn, B. H., H. W. Kroehl, Y. Kamide, and D. J. Gorney, Estimation of ionospheric electrodynamic prameters using ionospheric conductance deduced from Bremsstrahlung X-ray image data, *J. Geophys. Res.*, *94*, 2565–2586, 1989.

Akasofu, S.-I., Energy coupling between the solar wind and the magnetosphere, *Space Sci. Rev.*, *28*, 121–190, 1981.

Axford, W. I., and C. O. Hines, A unifying theory of high-latitude geophysical phenomena and geomagnetic storms, *Can. J. Phys.*, *39*, 1433–1464, 1961.

Baker, D. N., S.-I. Akasofu, W. Baumjohann, J. W. Bieber, D. M. Fairfield, E. W. Hones, B. Mauk, R. L. McPherron, and T. E. Moore, Substorms in the magnetosphere, *NASA Ref. Publ.*, *1120,* 1984.

Baker, D. N., T. I. Pulkkinen, M. Hesse, and R. L. McPherron, A quantitative assessment of energy storage and release in the Earth's magnetotail, *J. Geophys. Res.*, *102*, 7159–7168, 1997.

Bargatze, L. F., D. N. Baker, R. L. McPherron, and E. W. Hones Jr., Magnetospheric impulse response for many levels of geomagnetic activity, *J. Geophys. Res.*, *90*, 6387–6394, 1985.

Baumjohann, W., and Y. Kamide, Hemispherical Joule heating and the AE indices, *J. Geophys. Res.*, *89*, 383–388, 1984.

Codrescu, M. V., T. J. Fuller-Rowell, and J. C. Foster, On the importance of E-field variability for Joule heating in the high-latitude thermosphere, *Geophys. Res. Lett.*, *22*, 2393–2396, 1995.

Collier, M. R., J. A. Slavin, R. P. Lepping, A. Szabo, and K. Ogilvie, Timing accuracy for the simple planar propagation magnetic field structures in the solar wind, *Geophys. Res. Lett.*, *25*, 2509–2512, 1998.

Cooper, M. L., C. R. Clauer, B. A. Emery, A. D. Richmond, and J. D. Winningham, A storm time assimilative mapping of ionospheric electrodynamics analysis for the severe geomagnetic storm of November 8–9, 1991, *J. Geophys. Res.*, *100*, 19,329–19,342, 1995.

Elphinstone, R. D., J. S. Murphree, and L. L. Cogger, What is a global auroral substorm?, *Rev. Geophys.*, *34*, 169–232, 1996.

Emery, B. A., C. Lathuillere, P. G. Richards, R. G. Roble, M. J. Buonsanto, D. J. Knipp, P. Wilkinson, D. P. Sipler, and R. Niciejewski, Time dependent thermospheric neutral response to the 2–11 November 1993 storm period, *J. Atmos. Terr. Phys.*, *61*, 329–350, 1999.

Farrugia, C. J., F. T. Gratton, and R. B. Torbert, Viscous-type processes in the solar wind-magnetosphere interaction, *Space Sci. Rev.*, *95*, 443–456, 2001.

Frey, H. U., S. B. Mende, C. W. Carlson, J. C. Gérard, B. Hubert, J. Spann, R. Gladstone, and T. J. Immel, The electron and proton aurora as seen by IMAGE-FUV and FAST, *Geophys. Res. Lett.*, *28*, 1135–1138, 2001.

Galand, M., T. J. Fuller-Rowell, and M. V. Codrescu, Response of the upper atmosphere to auroral protons, *J. Geophys. Res.*, *106*, 127–139, 2001.

Germany, G. A., G. K. Parks, M. Brittnacher, J. Cumnock, D. Lummerzheim, J. F. Spann, L. Chen, P. G. Richards, and F. J. Rich, Remote determination of auroral energy characteristics during substorm activity, *Geophys. Res. Lett.*, *24*, 995, 1997.

Germany, G. A., G. K. Parks, M. J. Brittnacher, J. F. Spann, J. Cumnock, D. Lummerzheim, F. Rich, and F. G. Richards, Energy characterization of a dynamic auroral event using GGS UVI images, in *Geospace Mass and Energy Flow: Results From the International Solar-Terrestrial Physic Program*, *Geophys. Monogr. Ser.*, vol. 104, edited by J. L. Horwitz, D. L. Gallagher, and W. K. Peterson, p. 143, AGU, Washington, D. C., 1998a.

Germany, G. A., J. F. Spann, G. K. Parks, M. J. Brittnacher, R. Elsen, L. Chen, D. Lummerzheim, and M. H. Rees, Auroral observations from the Polar Ultraviolet Imager (UVI), in *Geospace Mass and Energy Flow: Results From the International Solar-Terrestrial Physic Program*, *Geophys. Monogr. Ser.*, vol. 104, edited by J. L. Horwitz, D. L. Gallagher, and W. K. Peterson, p. 149, AGU, Washington, D. C., 1998b.

Gonzalez, W. D., J. A. Joselyn, Y. Kamide, H. W. Kroehl, G. Rostoker, B. T. Tsurutani, and V. M. Vasyliunas, What is a geomagnetic storm?, *J. Geophys. Res.*, *99*, 5771–5792, 1994.

Ieda, A., S. Machida, T. Mukai, Y. Saito, T. Yamamoto, A. Nishida, T. Terasawa, and S. Kokubun, Statistical analysis of the plasmoid evolution with Geotail observations, *J. Geophys. Res.*, *103*, 4453–4465, 1998.

Imhof, W. L., et al., The Polar Ionospheric X-ray Imaging Experiment (PIXIE), *Space Sci. Rev.*, *71*, 385–408, 1995.

Kallio, E. I., T. I. Pulkkinen, H. E. J. Koskinen, A. Viljanen, J. A. Slavin, and K. Ogilvie, Loading-unloading processes in the nightside ionosphere, *Geophys. Res. Lett.*, *27*, 1627–1630, 2000.

Kan, J. R., L. Zhu, A. T. Y. Lui, and S.-I. Akasofu, A magnetosphere-ionosphere coupling theory of substorms including magnetotail dynamics, in *Auroral Physics*, edited by C.-L. Meng, M. J. Rycroft, and L. A. Frank, pp. 311–321, Cambridge Univ. Press, New York, 1991.

Knipp, D. J., et al., An overview of the early November 1993 geomagnetic storm, *J. Geophys. Res.*, *103*, 26,197–26,220, 1998.

Lepping, R. P., et al., The WIND magnetic field investigation, *Space Sci. Rev.*, *71*, 207–229, 1995.

Liou, K., P. T. Newell, C. I. Meng, M. Brittnacher, and G. Parks, Characteristics of the solar wind controlled auroral emissions, *J. Geophys. Res.*, *103*, 17,543–17,557, 1998.

Lu, G., D. Richmond, B. A. Emery, and R. G. Roble, Magnetosphere-ionosphere-thermosphere coupling: Effect of neutral winds on energy transfer and field-aligned current, *J. Geophys. Res.*, *100*, 19,643–19,659, 1995.

Lu, G., et al., Global energy deposition during the January 1997 magnetic cloud event, *J. Geophys. Res.*, *103*, 11,685–11,694, 1998.

Nisbet, J. S., Relations between the Birkeland currents, the auroral electrojet indices and high latitude Joule heating, *J. Atmos. Terr. Phys.*, *44*, 797–809, 1982.

Ogilvie, K. W., et al., SWE, A comprehensive plasma instrument for the WIND spacecraft, *Space Sci. Rev.*, *71*, 55–77, 1995.

Østgaard, N., J. Bjordal, J. Stadsnes, and E. Thorsen, PIXIE data processing at the University of Bergen, *Tech. Rep. 1999-05*, Univ. of Bergen, Bergen, Norway, 1999.

Østgaard, N., J. Stadsnes, J. Bjordal, R. R. Vondrak, S. A. Cummer, D. Chenette, M. Schulz, and J. Pronko, Cause of the localized maximum of X-ray emission in the morning sector: A comparison with electron measurements, *J. Geophys. Res.*, *105*, 20,869–20,884, 2000.

Østgaard, N., J. Stadsnes, J. Bjordal, G. A. Germany, G. K. Parks, R. R. Vondrak, S. A. Cummer, D. Chenette, and J. Pronko, Auroral electron distributions derived from combined UV and X-ray emissions, *J. Geophys. Res.*, *106*, 26,081–26,090, 2001.

Østgaard, N., R. R. Vondrak, J. W. Gjerloev, and G. A. Germany, A relation between the energy deposition by electron precipitation and geomagnetic indices during substorms, *J. Geophys. Res.*, *107*, 10.1029/2001JA002003, in press, 2002.

Parks, G. K., *Physics of Space Plasmas, Adv. Book Prog.*, 1st ed., Addison-Wesley, Reading, Mass., 1991.

Perrault, P., and S. I. Akasofu, A study of magnetic storms, *Geophys. J. R. Astron. Soc.*, *54*, 547, 1978.

Prigancova, A., and Y. I. Feldstein, Magnetospheric storm dynamics in terms of energy output rate, *Planet. Space Sci.*, *40*, 581–588, 1992.

Richmond, A. D., Global measures of ionospheric electrodynamic activity inferred from combined incoherent scatter radar and ground magnetometer observations, *J. Geophys. Res.*, *95*, 1061–1071, 1990.

Rostoker, G., Overview of observations and models of auroral substorms, in *Auroral Physics*, edited by C.-L. Meng, M. J. Rycroft, and L. A. Frank, pp. 257–272, Cambridge Univ. Press, New York, 1991.

Shue, J. H., J. K. Chao, H. C. Fu, C. T. Russell, P. Song, K. K. Khurana, and H. J. Singer, A new functional form to study the solar wind control of the magnetopause size and shape, *J. Geophys. Res.*, *102*, 9497–9511, 1997.

Siscoe, G. L., V. Formisano, and A. J. Lazarus, Relation between geomagnetic sudden impulses and solar wind pressure changes: An experimental investigation, *J. Geophys. Res.*, *73*, 4869–4874, 1968.

Spiro, R. W., D. H. Reiff, and J. L. J. Mather, Precipitating electron average flux and auroral zone conductance: An empirical model, *J. Geophys. Res.*, *87*, 8215–8227, 1982.

Stern, D. P., Energetics of the magnetosphere, *Space Sci. Rev.*, *39*, 193–213, 1984.

Sugiura, M., Hourly values of equatorial Dst for the IGY, in *Annual International Geophysical Year*, vol. 35, p. 9, Pergamon, New York, 1964.

Torr, M. R., et al., A far ultraviolet imager for the international solar-terrestrial physics mission, *Space Sci. Rev.*, *71*, 329–383, 1995.

Tsurutani, B. T., and W. Gonzalez, The efficiency of "viscous interaction" between the solar wind and the magnetosphere during intense northward IMF events, *Geophys. Res. Lett.*, *22*, 663–666, 1995.

Tsurutani, B. T., J. A. Slavin, Y. Kamide, R. D. Zwickl, J. H. King, and C. T. Russell, Coupling between the solar wind and the magnetosphere: CDAW 6, *J. Geophys. Res.*, *90*, 1191–1199, 1985.

Zwickl, R. D., L. F. B. D. N. Baker, C. R. Clauer, and R. L. McPherron, An evaluation of the total magnetospheric energy output parameter, U_T, in *Magnetotail Physics*, edited by A. T. Y. Lui, pp. 155–159, Johns Hopkins Univ. Press, Baltimore, Md., 1987.

N. Østgaard and R. R. Vondrak, Laboratory for Extraterrestrial Physics, Code 690, Building 2, NASA/GSFC, Greenbelt, MD 20771, USA. (ostgaard@lepvax.gsfc.nasa.gov)

G. Germany, Center for Space Plasma and Aeronomy Research, University of Alabama in Huntsville, Huntsville, AL 35899, USA.

J. Stadsnes, Department of Physics, University of Bergen, N-5007, Bergen, Norway.